Electrochimica Acta 54 (2009) 3766–3774

Contents lists available at ScienceDirect

Electrochimica Acta

journal homepage: www.elsevier.com/locate/electacta

Ionic double layer of atomically flat gold formed on mica templates

Terry C. Chilcott[a,*], Elicia L.S. Wong[a,b], Hans G.L. Coster[a], Adelle C.F. Coster[c], Michael James[b]

[a] Biophysics and Bioengineering, School of Chemical and Biomolecular Engineering, University of Sydney, City Road, Sydney, NSW 2008, Australia
[b] Australian Nuclear Science and Technology Organisation, Lucas Heights Research Laboratory, Lucas Height, NSW 2234, Australia
[c] School of Mathematics and Statistics, University of New South Wales, Sydney, NSW 2052, Australia

ARTICLE INFO

Article history:
Received 27 August 2008
Received in revised form 15 January 2009
Accepted 24 January 2009
Available online 3 February 2009

Keywords:
Ionic double layer
Impedance
Surface topography
AFM
EIS
CPE

ABSTRACT

Electrical impedance spectroscopy characterisations of gold surfaces formed on mica templates in contact with potassium chloride electrolytes were performed at the electric potential of zero charge over a frequency range of 6×10^{-3} to 100×10^{3} Hz. They revealed constant-phase-angle (CPA) behaviour with a frequency exponent value of 0.96 for surfaces that were also characterised as atomically flat using atomic force microscopy (AFM). As the frequency exponent value was only marginally less than unity, the CPA behaviour yielded a realistic estimate for the capacitance of the ionic double layer. The retention of the CPA behaviour was attributed to specific adsorption of chloride ions which was detected as an adsorption conductance element in parallel with the CPA impedance element. Significant variations in the ionic double layer capacitance as well as the adsorption conductance were observed for electrolyte concentrations ranging from 33 μM to 100 mM, but neither of these variations correlated with concentration. This is consistent with the electrical properties of the interface deriving principally from the inner or Stern region of the double layer.

1. Introduction

Detailed structural analysis of organic layers adsorbed to or self-assembled on metallic substrates such as gold have become the subject of much interest as a consequence of their potential application as biological, and other types of sensors, e.g. [1–5]. Invariably the analyses of the layers and their performance as sensors are hampered by the interface that forms between the ionic/biological environment and the substrate. This is because the interfacial impedance is at best comparable in magnitude to the impedance of the organic layers and disperses with frequency in a complicated manner that is dependent on interfacial topography and the adsorption of chloride ions which are ubiquitous in biological environments. The properties of the interface are modified through the attachment of the organic layers and, subsequently, by the binding of the targeted molecules to these layers. An understanding of the way in which surface topography, i.e. roughness, chloride adsorption, the self-assembly of monolayers and the sensing events modulate the interfacial impedance is crucial to the design of practical biosensors. The fundamentals of this problem has been under investigation for over a 100 years and in recent times has been the subject of investigations that has shed new light on this old problem (e.g. [6–20]).

1.1. Electrode–electrolyte interface—the constant-phase-angle (CPA) impedance element

The measured electrical impedance of a metal electrode of arbitrary roughness immersed in an electrolyte and in which no charge passes between the electrode and electrolyte, has been commonly described, for frequencies typically greater than 0.1 Hz (e.g. [21]), by the function:

$$z_T(\omega) = Z_e + A(j\omega)^{-n} \tag{1}$$

where Z_e represents the area specific impedance of the electrolyte, $A(j\omega)^{-n}$ the area specific impedance of the electrode–electrolyte interface, ω the angular frequency and $j \equiv \sqrt{-1}$.

The identity $j = e^{j(\pi/2)}$ transforms the function representing the impedance of the electrode–electrolyte into a polar form, specifically:

$$A(j\omega)^{-n} = A\omega^{-n}\, e^{j(-n(\pi/2))}$$

from which the magnitude and phase angle of the function are readily deduced as

$$|A(j\omega)^{-n}| = A\omega^{-n} \quad \text{and} \quad \angle(A(j\omega)^{-n}) = -n\frac{\pi}{2}, \quad \text{respectively.}$$

This transformation reveals that the phase angle of $A(j\omega)^{-n}$ is constant in ω, thus providing the common nomenclature for this impedance as the constant-phase-angle (CPA) impedance element.

* Corresponding author. Tel.: +61 408463761.
E-mail address: t.chilcott@usyd.edu.au (T.C. Chilcott).

0013-4686/$ – see front matter. Crown Copyright © 2009 Published by Elsevier Ltd. All rights reserved.
doi:10.1016/j.electacta.2009.01.069

The CPA impedance element also can be expressed as follows:

$$Z_{cpa} \equiv A(j\omega)^{-n} \equiv \frac{1}{g_{cpa} + j\omega c_{cpa}} \quad (2)$$

where g_{cpa} and c_{cpa} are frequency dependent conductance and capacitance functions. Appropriate transformations of Eq. (2) yield the following expressions for g_{cpa} and c_{cpa}:

$$c_{cpa}(\omega) = A^{-1}\omega^{n-1} \sin\left(n\frac{\pi}{2}\right) \quad \text{and} \quad g_{cpa}(\omega) = A^{-1}\omega^{n} \cos\left(n\frac{\pi}{2}\right) \quad (3)$$

1.2. Additions to the CPA impedance element attributed to ionic adsorption

For situations when charge passes between the electrode and electrolyte, an impedance element $Z_{adsorption}$ that effectively shunts the CPA impedance, has been introduced into Eq. (1) to describe the measured electrical impedance of a metal electrode of arbitrary roughness immersed in an electrolyte, yielding the following expression for the total impedance of the system (for frequencies typically greater than 0.1 Hz, e.g. see [22]):

$$z_T(\omega) = Z_e + \frac{1}{(1/Z_{adsorption}) + (1/Z_{cpa})} \quad (4)$$

The simplest circuit representation of $Z_{adsorption}$ is a conductor in series with a capacitor (e.g. see [23] and [24]) but, unlike the conductive and capacitive components for Z_{cpa} (see Eq. (3)) are constants in ω. However, a 'Warburg' component with a frequency dependency similar to that of Z_{cpa} (but with $n = 1/2$) is introduced in series with these components to account for adsorption when driven by anionic diffusion (e.g. see [25–27]).

1.3. Modelling the bulk electrolyte

The impedance of the bulk electrolyte is well characterised by the Maxwell–Wagner model which is given by

$$Z_e \equiv \frac{1}{g_e + j\omega c_e} \quad (5)$$

where g_e is the conductance per unit area and c_e the capacitance per unit area of the electrolyte. In contrast to the CPA impedance element, the conductance and capacitance of the electrolyte are defined by bulk electrical and geometrical properties that are constants in ω. Specifically, for a layer of electrolyte of thickness d_e, conductivity σ_e and dielectric permittivity ε_e:

$$g_e \equiv \frac{\sigma_e}{d_e} \quad \text{and} \quad c_e \equiv \frac{\varepsilon_e}{d_e} \quad (6)$$

1.4. Physical origins of the constant-phase-angle (CPA) element

The physical origins of the capacitive and conductive components of the CPA element and further embellishments have proven more illusive. The possible exception is for the special case when the frequency exponent $n = 1$ whence Eqs. (2) and (3) yield $g_{cpa} = 0$ and $c_{cpa} = A^{-1}$. That is, the impedance of the CPA element becomes that of a Maxwell–Wagner capacitor, the physical properties of which have been purported to derive from dielectric and geometrical properties of an ionic double layer of uniform thickness on an ideally flat metal surface in which no charge passes between the electrode and electrolyte (i.e. $Z_{adsorption} = \infty$). The manifestation of the dependence of the CPA capacitance on frequency (Eq. (3)) for decreasing values of n has been generally correlated with increasing roughness of the electrode surface (e.g. [13]).

Several models that consider the electrical properties of the electrolyte, the non-transference of charge at the interface and surface topography have been devised to explain the commonly observed CPA behavior of electrode–electrolyte interfaces of varying roughness. That proposed by de Levie [13] for a mechanically polished electrode assumed that the surface contained V-shaped groves, the impedance of which was represented by tapered transmission lines. This model yielded a CPA element that was restricted to using a frequency exponent of $n = 1/2$. Wang and Bates [28] generalised de Levie's model to yield values for n close to those observed experimentally (typically $0.7 < n < 0.9$). Le Mehaute and Crepy [29] proposed a surface topography based on fractal branching. Although criticised by Keddam and Takenouti [30], Liu [31,32] showed that fractal branching yielded CPA behaviour.

1.5. Predictions of fractal modelling for surfaces approaching atomic roughness (effects of mono-atomic terraces)

Liu's fractal model is shown in Fig. 1 and its derivation is outlined in Appendix A. Dispersions of the total conductance and capacitance with frequency for the fractal model are shown in Fig. 2 as a function of the number of fractal branches N, which has been

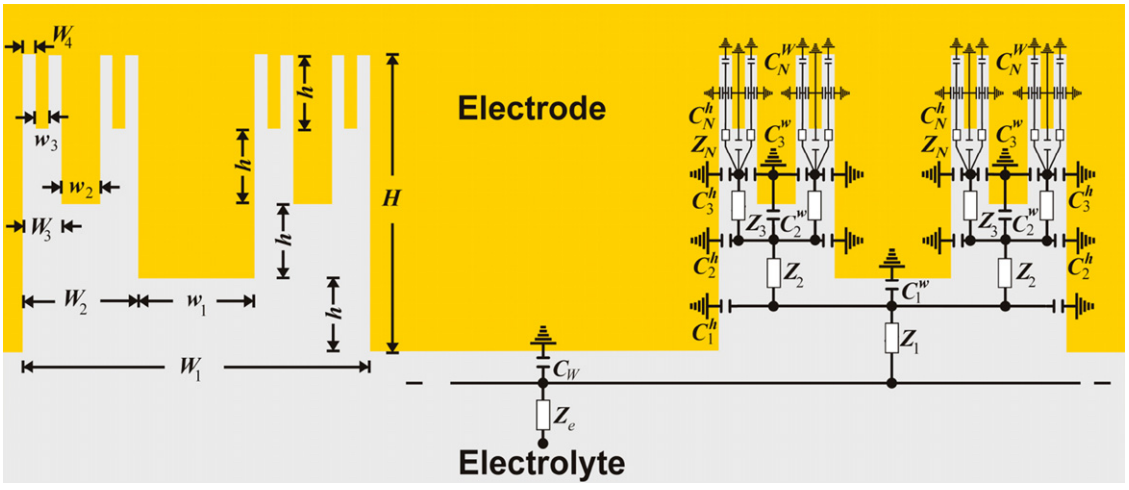

Fig. 1. Fractal (Cantor bar) model for the interface between an electrolyte and an electrode with a rough surface. The surface is modelled as groves with many stages of branching. Only two groves with four stages of branching are shown. The variables denoting the dimensions and components of the equivalent circuit are also shown.

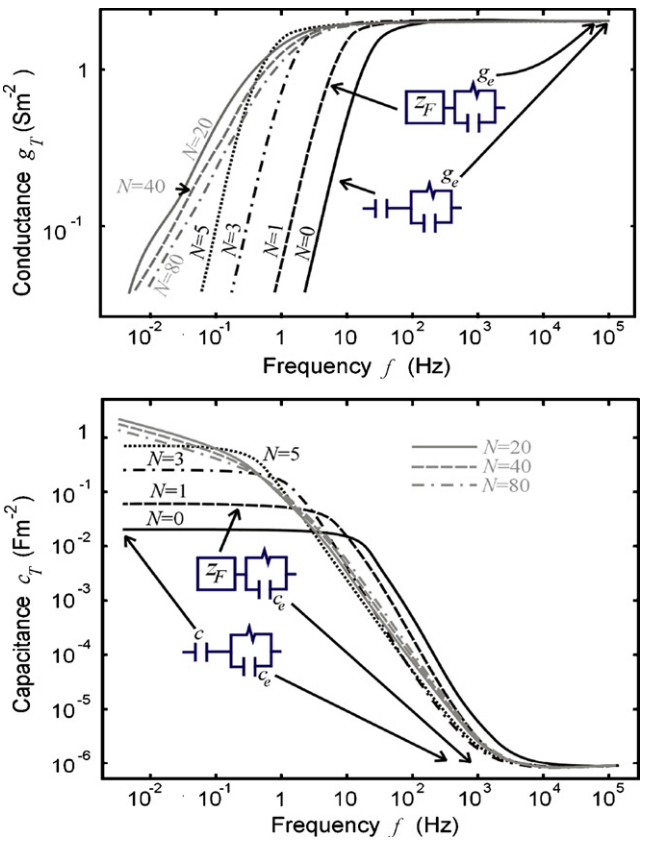

Fig. 2. Theoretical conductance and capacitance spectra based on Liu's Cantor bar fractal model shown in Fig. 1 for atomically flat ($N=0$) and rough ($N>1$) surfaces in contact with a 100 μM electrolyte of conductance g_e and capacitance c_e. Parameters for the flat surface are: $c=20\,\mathrm{mF\,m^{-2}}$; $g_e=2\,\mathrm{S\,m^{-2}}$ and $c_e=0.9\,\mu\mathrm{F\,m^{-2}}$. Those for the rough surfaces are $c=20\,\mathrm{mF\,m^{-2}}$; $g_e=2\,\mathrm{S\,m^{-2}}$ and $c_e=0.9\,\mu\mathrm{F\,m^{-2}}$; $a=10$; $H=38$ nm and $W=20$ nm.

arbitrarily chosen as a parameter that generally correlates with roughness.[1]

The dispersion for an atomically flat surface corresponds to $N=0$ revealing that the total capacitance plateaus to a value at low frequencies which is approximately the capacitance c for the ionic double layer of constant thickness on a flat surface, and a value at high frequencies which is approximately the dielectric/geometrical capacitance c_e of the electrolyte. The conductance at low frequencies increases with increasing frequency and plateaus at high frequencies to a value which is approximately the geometrical conductance g_e of the electrolyte. Eq. (3) shows that the absence of a dispersion of the capacitance with frequency at low frequencies correlates with a CPA frequency exponent value of unity, i.e. $n=1$.

The presence of extensive numbers of mono-atomic terraces over an otherwise atomically flat surface can also be modelled using $N=1$. However, Fig. 2 reveals a CPA frequency exponent value of unity for this situation as well[2] and for more extensive terracing corresponding to $N=3$ and 5.

[1] Other fractal parameters, such as the width W, length L and height h high of the groves at the surface and the fractal scaling factor a that determines the degree to which groves diminish in size with each fractal branch also define surface roughness.

[2] Note that the modeling greatly overestimates the height h of the terracing (see caption to Fig. 2) yet a CPA exponent of unity prevails in the dispersions of the capacitance with frequency.

1.6. Predictions of CPA behaviour for rough surfaces

For the fractal model of a non-flat surface, the commonly observed CPA capacitance–frequency and conductance–frequency characteristics described by Eq. (3) are revealed in the low-frequency regime at relatively large values of N (e.g. Fig. 2 for $N>20$). The slopes of the characteristics yield values for the CPA frequency exponent n that are typical of rough surfaces, i.e. $0.7<n<0.9$. However, the slopes (i.e. n) can be seen to be insensitive to variations in N for values ranging from 20 to 80, that is, for fractal surfaces covering a broad range of roughness. A consequence of this is that n will be similarly insensitive to other fractal parameters, defined in Fig. 2. This is consistent with studies of Bates et al. [21] and later Pajkossy [33] who showed experimentally that a unique relationship between the fractal dimension of fractal models and the CPA exponent n could not be established for metal–electrolyte systems.

Geometrical models of this type could be applicable to surfaces characterised as very rough [34] and whose CPA characteristics exhibit dependencies on geometrical parameters at measurable frequencies (e.g. $>10^{-3}$ Hz).

1.7. CPA behaviour of atomically flat gold–electrolyte surfaces

Significant progress has been made by Pajkossy et al. [19] in characterising the electrochemistry of the gold–electrolyte interface. They report a value for the CPA exponent n of 0.99 for single-crystal electrodes in the absence of specific ionic adsorption. Such behaviour is consistent with both CPA characteristics described by Eq. (3), which predicts ideal capacitive behaviour for $n\approx1$ and Liu's fractal model which also predicts $n=1$ for $N=0$ (see Fig. 2).

However, Pajkossy et al. report the persistence of CPA-behaviour and a decrease in n in the presence of specific ionic adsorption. The capacitance and conductance dispersions for fractal model shown in Fig. 2 do not predict this behaviour even for surfaces with mono-atomic terraces (i.e. for $5>N>0$).

1.8. Scope of present study

Electrical impedance characterisations are presented here on gold–electrolyte interfaces whose surface topologies were characterized using atomic force microscopy (AFM). One of the topographies was characterised as atomically flat and provided an opportunity to study the electrochemical properties of the gold–electrolyte interface as a function of electrolyte concentration unencumbered by the complication of surface topography but over a frequency range extending down close to 10^{-3} Hz.

2. Materials and methods

2.1. Materials

Gold wire with 1 mm diameter (99.999% purity) and silver wire with 1 mm diameter (99.99% purity) were purchased from Aldrich Chemicals (Sydney, NSW, Australia). Reagent grade potassium chloride was purchased from Aldrich Chemicals (Sydney, NSW, Australia). Absolute ethanol was purchased from Ajax (Sydney, Australia). All the chemicals were used as received without further purification. Milli-Q (18 MΩ cm) was used for the rinsing and preparation of solutions.

2.2. Preparation of flat gold surface

Evaporated gold on a mica template was obtained from School of Chemistry, Physics and Earth Science, Flinders University (Adelaide, SA, Australia) where the gold evaporation was performed using the procedure described previously [35]. The mica-supported gold

was glued to a microscope glass slide using Torr Seal® (Varian Vacuum Products, Lexington, MA, USA) to produce a mica–gold–glass support sandwich type of assembly. After 24 h the Torr Seal had attached firmly to the mica–gold pieces. The sandwich was placed in liquid nitrogen to cryogenically cleave away the mica and expose the atomically flat gold surface. The atmospheric water condensate on the flat gold substrate was removed by blowing a stream of dry nitrogen onto the substrate.

2.3. AC impedance spectroscopy

AC impedance measurements were performed using an InPhaze Spectrometer [36] and characterisation chamber [37] (InPhaze Pty. Ltd., Sydney, Australia). The spectrometer provided a magnitude resolution of 0.002% and phase angle resolution of 0.001° over a frequency range of 6 mHz to 100 kHz.

Fig. 3(a) is a schematic of the characterisation chamber which features a circular compressible gasket of rectilinear cross-section that provided an accurate estimate of the active area of measurement (i.e. 1.81×10^{-5} m^2). The rectilinear gasket also avoided spatial distortions of the alternating current I used for impedance measurements that would have occurred using an o-ring gasket. Such distortions in themselves have been shown to manifest CPA-like characteristics (see appendix of [2]). Also featured is a very low-leak reference electrode (type LF-2 from Innovative Instruments Inc. 8533 Queen Brooks Ct.Tampa, FL 33637, USA) located in an electrolyte filled recess. This was used to measure the electrical potential response V of the electrolyte–gold interfaces[3] to the current stimulus I. The chamber also featured a mechanism involving three identical springs of low-spring constant (not shown) for applying a uniform pressure to seal the gasket over the active area while minimising deformation of the gold surfaces.

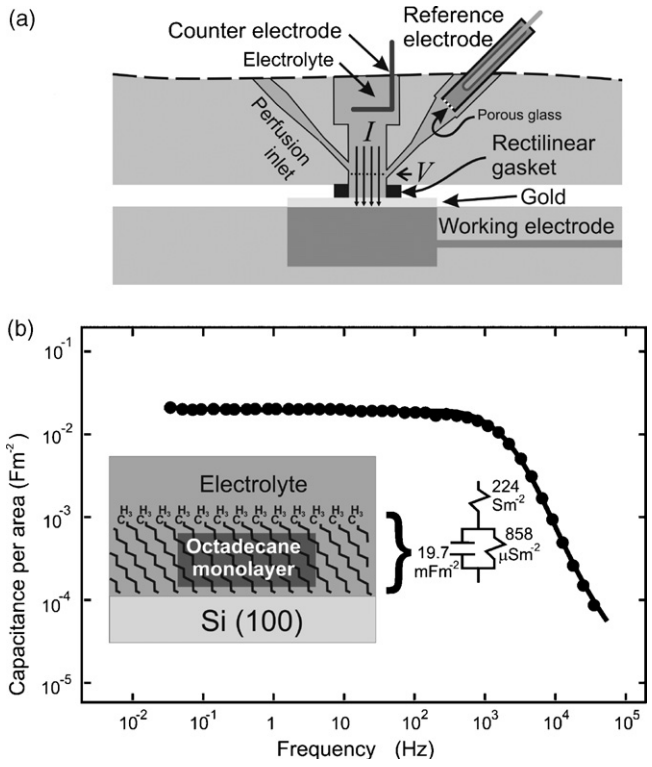

Fig. 3. (a) Schematic of the experimental chamber used for characterising the gold surfaces. The rough gold sample was placed directly on top of the working electrode as shown. As the flat gold surface was supported on an insulating microscope slide, it was necessary to attach a silver wire (not shown) to the non-active area of the gold surface with conducting glue. In this instance, the silver wire served as the working electrode. (b) Capacitance measurements (●) obtained for an octadecane monolayer attached to a highly doped atomically flat silicon wafer placed in the chamber shown in (a)—adapted from [2]. The two-element Maxwell–Wagner model that was fitted to the measurements is also shown. One element represented the electrolyte of conductance 224 S m^{-2} and the other element the monolayer of conductance 858 μS m^{-2} and capacitance 19.7 mF m^{-2}. The constancy of the measured capacitance over five decades of frequency below 10^2 Hz (originating principally from the capacitive properties of the monolayer) is consistent with that expected for an atomically flat surface, i.e. a value for the constant-phase-angle (CPA) exponent n of unity.

The current I was injected into the system via an attenuating circuit of high impedance (typically 1 MΩ) and a know impedance standard of similarly high impedance. No bias signals were applied to the system such as would be the case with a potentiostat that utilises high-gain feedback circuitry to regulate the amplitudes of both the alternating and biasing signals. The alternating voltage responses of the system and the impedance standard were typically less than 40 mV in amplitude. A least-squares fitting of sinusoidal functions to the measured responses together with the known values for the standard provided accurate estimates of the impedance magnitude and phase of the system as well as the bias current. The average bias current during the acquisition of some 10 spectra over a period of some 12 h was typically zero indicating that the electrical potential of the interface was that for zero charge.

The suitability of the chamber for impedance characterisation of surface roughness is illustrated in Fig. 3(b) which shows the absence of CPA behaviour of an organic layer on atomically flat silicon(1 0 0) in the low-frequency range where such behaviour has been commonly reported for metal–electrolyte interfaces [2]. Impedance measurements at very high frequencies (typically >1 kHz) yielded frequency independent estimates of the area specific conductance of the electrolyte, i.e. g_e, and estimates of the area specific capacitance,[4] i.e. c_e (see Eq. (5)). Assuming that the dielectric constant for the electrolyte was approximately 79 then Eq. (6) yielded estimates of the thickness of electrolyte involve in the measurement that were consistent with the known height of the recess above the interface. Conductivity estimates for the electrolytes based on Eq. (6) were also consistent with published values for the conductivity of potassium chloride electrolytes (CRC Handbook of Chemistry and Physics [38]).

Impedance spectra are presented as capacitance (i.e. $c_T = \mathrm{Im}[1/z_T]/\omega$) and conductance (i.e. $g_T = \mathrm{Re}[1/z_T]$) dispersions with frequency. Variations of the imaginary capacitance (i.e. g_T/ω) as a function of the real capacitance (i.e. c_T) are also presented.

2.4. Statistical analysis of models

A least-squares-error method was employed to fit models to the averaged impedance spectra. Specifically the method minimised:

$$\text{Reduced-}\chi^2 \equiv \frac{\chi^2}{N - N_f} \quad \text{where} \quad \chi^2 \equiv \sum_{n=1}^{N} \left(\frac{m_n - f(\omega_n)}{\sigma_n} \right)^2 \qquad (7)$$

[3] The high-input impedance of the amplifier (10^{12} Ω) used to measure the electrical potential at the tip of the reference electrode in the InPhaze chamber ensured that the amplifier drew negligibly small current from the electrolyte–gold interfaces. Thus from Ohms law the tip of the reference electrode was effectively at the same electric potential as that at the entry to the recess, i.e. V in Fig. 3(a). The aperture of the entry was very small so as to minimise the spatial distortion of the alternating current I in the plane that extends parallel to the interface from the entry into the electrolyte (dotted line in Fig. 3(a)). Thus the reference electrode measured the electrical potential response of the interfaces (V) to the current stimulus I *independently* of the position or the orientation of the reference electrode within the recess.

[4] For concentrations typically less than 10 mM.

and where $f(\omega)$ is the model function containing N_f adjustable parameters and m_n and σ_n are the mean and standard deviation, respectively, of the nth of N measurements.

2.5. Atomic force microscopy (AFM)

All AFM measurements were acquired in tapping mode in air with a Dimension 3000 (Digital Instruments) using commercially modified Si_3N_4 cantilevers. Several images were taken such that the parameters of force, tip frequency, scan size, and scanning speed could be optimally adjusted for best imaging. All measurements were performed at room temperature and the laser used for detecting the cantilever deflection had a minimal effect on the temperature of the sample under the cantilever. The height distribution was determined by cross-section analysis using the default Digital Instruments (Version 4.31, Rev B.) software.

3. Results

3.1. Atomic force microscopy (AFM) images

A representative high-resolution AFM height image (tapping mode in air) and its corresponding cross-section profile for the atomically flat gold surfaces formed on mica templates are shown in Fig. 4. The height image and profile showed uniform topography with small circular structures displaying a wave-like feature across the surface with amplitude of 0.2 nm and a diameter of up to ~40 nm. The flat gold surfaces were found to produce regions of up to 40,000 nm^2 with root mean square roughness of 0.002 nm.

The flatness of the surface was confirmed through a roughness analysis which yielded average roughness values of R_{rms} of 0.11 ± 0.02 nm, R_a of 0.084 ± 0.02 nm and R_{max} of 1.10 ± 0.1 nm for a

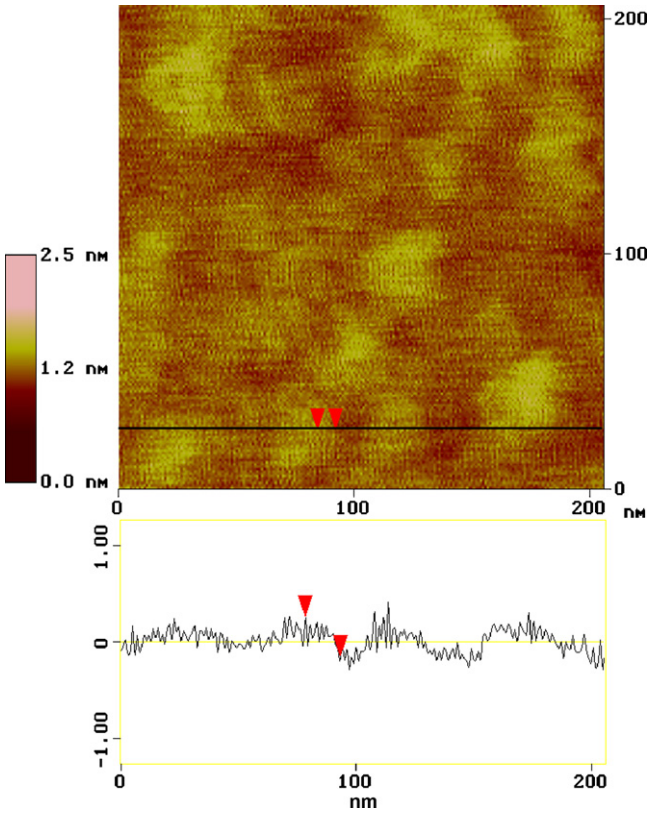

Fig. 4. AFM image of flat gold.

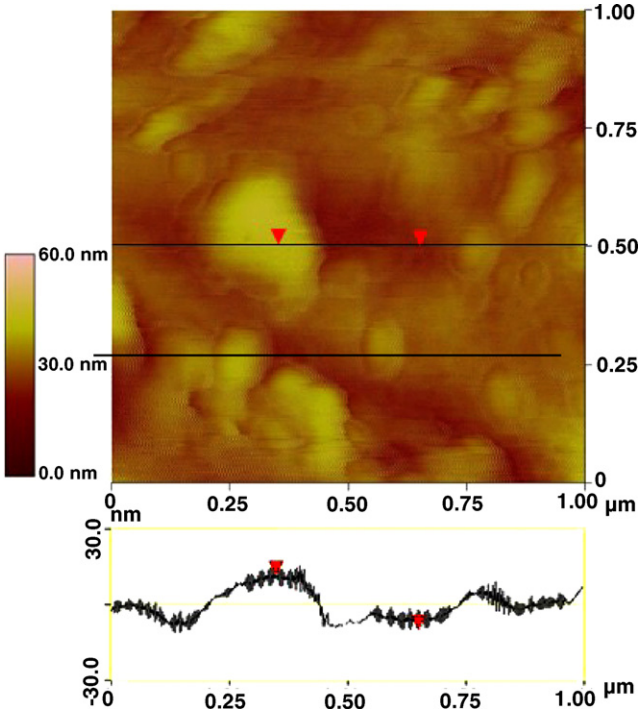

Fig. 5. AFM image of rough gold.

200 nm × 200 nm area. These observations are in accordance with previous AFM studies on flat gold surfaces; e.g. [39–43].

The representative AFM topographical image of the rough gold surface and its height profile are shown in Fig. 5.

In contrast to the atomically flat gold sample, the height image of the rough gold substrate shows features akin to a nanoscale moonscape. The maximum height difference (R_{max}) over a 1 µm × 1 µm area for this sample was 34 ± 1 nm. The average roughness values for this surface were R_{rms} of 4.7 ± 0.2 nm and R_a of 3.7 ± 0.3 nm, of order 40 times rougher than the flat gold samples.

3.2. Impedance measurements

Fig. 6 compares the measured dispersions of the conductance and capacitance with frequency of a 33.3 µM KCl electrolyte in contact with surfaces whose AFM images are shown in Figs. 4 and 5. At high frequencies the conductance and capacitance plateaux to yield the approximate bulk conductance and capacitance values for the electrolyte, i.e. $g_e \approx 2\,S\,m^{-2}$ and $c_e \approx 0.8\,\mu F\,m^{-2}$, whereas at low frequencies, the capacitance plateaus to yield approximate bulk conductance and capacitance values similar in magnitude to those obtained for interfaces of polycrystalline and single crystal gold surfaces under similar biasing conditions [20].

Fig. 6 shows that the capacitance measurements disperse with frequency in the manner described by Eq. (3) which characterises CPA behaviour. The capacitance loci of these measurements are shown in Fig. 7 and are similar in form to those obtained previously for polycrystalline gold [44]. The measurements yield estimates of the CPA frequency exponent n of approximately 1 and 0.8 for topographies characterised as flat (□) and rough (■), respectively. These values are broadly consistent with the respective AFM characterised topographies shown in Figs. 4 and 5 and for topographies of metal–electrolyte interfaces reported in the literature (e.g. [21]) including gold interfaces approaching atomic flatness (e.g. [45] and [19]).

3.3. Modelling the impedance measurements

The theoretical curves fitted to the conductance and capacitance measurements shown in Figs. 6 and 7 were generated by Eq. (4) which can be readily derived from the model circuit shown in Fig. 7(c). The model circuit includes a conductance element g_{ad} in parallel with the obligatory CPA impedance element, connected in series with the Maxwell–Wagner impedance element representing the electrolyte.

A closer inspection of the capacitance dispersion with frequency for the atomically flat surface (□, Fig. 6(c)) reveals the persistence of CPA characteristics with an exponent value of 0.96, that is, close to unity. Exponent values approaching unity are consistent with interfacial studies of atomically flat electrodes in contact with electrolytes free of ions, such as chloride ions, that adsorb to gold [27]. The theoretical curves representing such an ideal, chemically inert flat metallic surface, are shown in Figs. 6 and 7 as dashed curves and correspond to an interface represented by a simple capacitor (i.e. $g_{ad} = g_{cpa} = 0$ and c_{cpa} = constant). However, whilst the CPA element was sufficient to explain the dispersions of capacitance it was necessary to include an adsorption conductance element g_{ad} in the model (see Fig. 7(c)) to explain the dispersion of the conductance for both flat (□) and rough (■) surfaces.

3.4. Dependencies of c_{cpa} and g_{ad} on electrolyte concentration

Experiments and analyses were performed on the atomically flat surface in contact with potassium chloride electrolytes of concentrations ranging from 33 μM to 100 mM. The general features

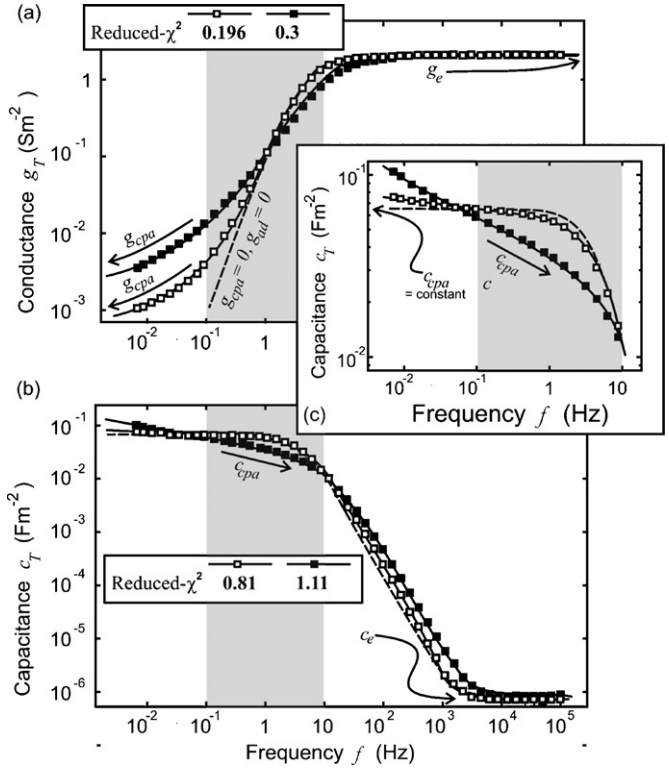

Fig. 6. Conductance (a) and capacitance (b and c) spectra for flat (□) and rough (■) gold surfaces in contact with a 33.3 μM electrolyte (average standard deviation for 10 spectra = 0.5%). The full curves are theoretical curves based of the model shown in Fig. 7(c) fitted to the conductance and capacitance spectra (see Fig. 7(b) for model parameter values). The shaded areas identify the frequency domain where constant-phase-angle (CPA) characteristics have been generally observed for electrolyte–metal interfaces. The dashed curve is that for an ideally flat surface in which interfacial properties derive from capacitive properties of the ionic double layer that are independent of angular frequency ω.

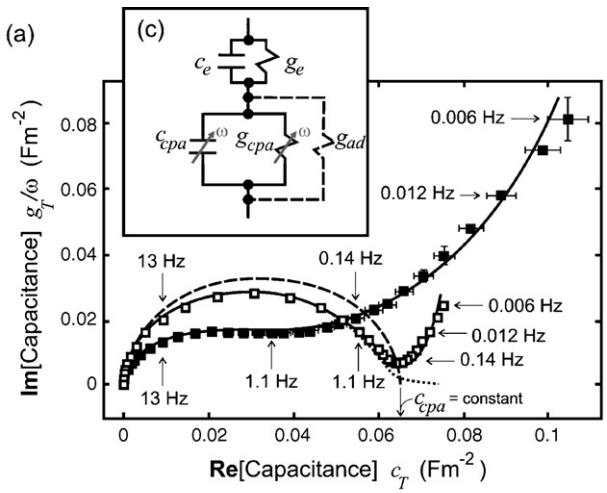

(b)

c_{cpa} (Fm^{-2})	0.065 x $\omega^{-0.04}$	0.055 x $\omega^{-0.19}$	0.065 x $\omega^{-0.19}$	0.065
g_{cpa} (Sm^{-2})	0.0041 x $\omega^{0.96}$	0.018 x $\omega^{0.81}$	0.0	0.0
g_{ad} (Sm^{-2})	0.00080	0.0021	0.0	0.0
c_e (μFm^{-2})	0.700	0.861	0.680	0.680
g_e (Sm^{-2})	2.00	1.84	2.00	2.00
Reduced-χ^2	0.83	1.15	20.3	22.2

Fig. 7. (a) Capacitance plot of the conductance and capacitance spectra shown in Fig. 6 for flat (□) and rough (■) gold surfaces in contact with a 33.3 μM electrolyte. (b) Parameter values for the model (c) fitted to the spectra and values for other theoretical curves assuming that the interfacial properties derive from capacitive properties of the ionic double layer that are either dependent (dotted curve) of independent (dashed curve) of angular frequency ω.

of the conductance and capacitance dispersions with frequency attributable to these ionic interfaces were similar to those dispersions shown in Figs. 6 and 7 for the flat surface (□) in contact with an electrolyte of 33 μM concentration. This was also reflected in the detailed analyses of these dispersions which yielded CPA exponent and conductance values that were similar in magnitude to those values obtained for the 33 μM concentration, i.e. $n = 0.96$ and $g_{cpa} = 4.1 \times \omega^{0.96}$ mS m^{-2}.

The detailed analyses further revealed variations in the values obtained for the CPA capacitance c_{cpa} and the adsorbent conductance g_{ad}, which are plotted as a function of electrolyte concentration in Fig. 8. Whilst the variations in the values obtained for c_{cpa} and g_{ad} are substantial, linear regression analyses (dotted curves in Fig. 8) revealed poor correlations of these variations with concentration. The average values for c_{cpa} and g_{ad} were found to be $66 \times \omega^{-0.04}$ mF m^{-2} and 1.3 mS m^{-2}, respectively.

4. Discussion

The electrical impedance spectroscopy (EIS) and atomic force microscopy (AFM) characterisations of rough and flat gold surfaces presented here yield results consistent with similar studies on polycrystalline and single crystal gold surfaces reported in the literature.

Whilst the measurements for the atomically flat surface (□, Fig. 6(c)) approached those for a chemically inert flat surface at high frequencies (dashed curve) they diverge increasingly with decreasing frequency. This divergence from ideal constant capacitive behaviour could not be attributed to surface topography as AFM images (Fig. 4) characterised the topography as close to atomically flat for which the fractal model predicts ideal capacitive characteristic (e.g. see theoretical curves in Fig. 2 for $N = 0$). It is also unlikely to be attributed to mono-atomic terracing [46] for which the fractal

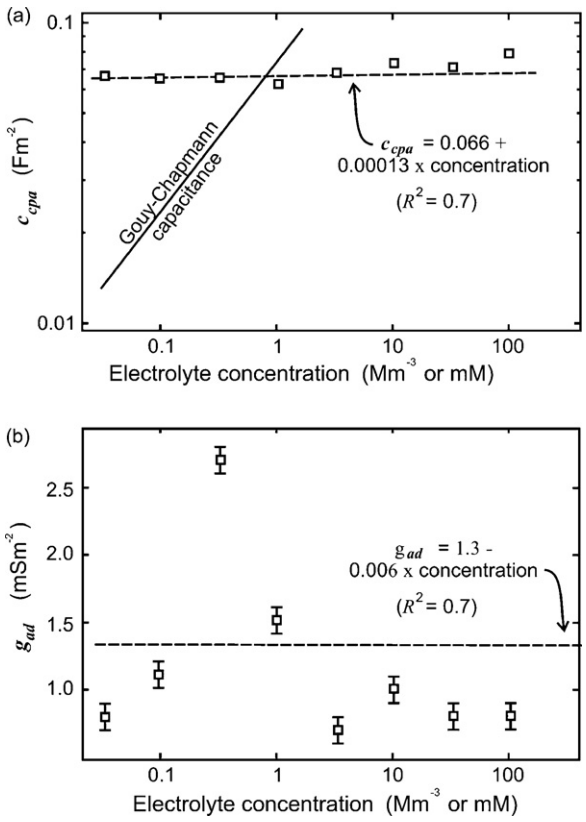

Fig. 8. (a) Dependence of the constant-phase-angle (CPA) capacitance c_{cpa} on electrolyte concentration. The Gouy-Chapmann capacitance is given by Eq. (8) and is proportional to the square root of the concentration. (b) Dependence of the adsorbent conductance g_{ad} on electrolyte concentration.

model also predicts ideal capacitive characteristics (e.g. see Fig. 2 for $5 > N > 0$).

It would thus appear likely that the retention of capacitance (CPA) dispersions on atomically flat surfaces should be attributed to anionic adsorption occurring in the interface, which is consistent with earlier findings of Pajkossy et al. [27] and their conclusion that it is due to "surface disorder (i.e. heterogeneities on the atomic scale) rather than roughness (i.e. geometric irregularities much larger than those on the atomic scale)" [47] and "specific adsorption and/or adsorption-related processes" [27].

The EIS studies on rough surfaces reveal CPA characteristics similar to those predicted by the geometrical fractal model [31] (cf. Fig. 2, Fig. 5 and ■, Fig. 6). This would suggest that such "geometric models might be applicable for interpreting impedance spectra of high-surface area (porous) electrodes" [20].

The value of 0.96 obtained for the CPA exponent n in the present study for the mica templated gold in contact with electrolytes containing adsorbent chloride ions is only marginally less than the exponent value of 0.99 obtained for single crystal surfaces in contact with electrolytes containing non-adsorbent ions [27]. It would thus appear that the electrolyte interface of atomically flat surfaces, i.e. the ionic double layer, "behaves as an ideal capacitor in the absence of specific adsorption" [27].

The adsorption conductance element g_{ad} was a necessary inclusion in the model (Fig. 7(c)) for obtaining statistically justifiable fits to the conductance dispersions at low frequencies (i.e. reduced-$\chi^2 \approx 1$) for both flat (□) and rough (■) surfaces. However, the reduced-χ^2 values could not justify the inclusion of an adsorption capacitor. Nonetheless, the inclusion of g_{ad} and a CPA exponent less than the value of 0.99 obtained for atomically flat surface in the absence of specific adsorption, were sufficient indicators that chloride adsorption was occurring at these surfaces.

The deduced values for g_{ad} were 0.8 mS m^{-2} for the flat surface (□, Fig. 7(b)) and 2.1 mS m^{-2} for the rough surface (■, Fig. 7(b)) indicated that adsorption was largest for the rougher surface. This is consistent with the rougher topography providing the larger surface area for chloride adsorption.

The EIS studies presented here further reveal that the adsorption conductance for the atomically flat surface, which can be attributed to Faradic transferences of chloride ions between the electrolyte and the gold, was independent of concentration (see Fig. 8(b)). An initial expectation is that this Faradaic conductance might be strongly correlated to concentration as it would be attributable to a diffusion driven adsorption covering a 300-fold range in concentration. A consequence of this expectation is that the capacitance of the double layer might be correlated to concentration. However, Fig. 8(a) reveals a poor correlation with even less scatter than then results for the Faradaic conductance.

These observations have implications regarding the origin of the ideal capacitive behaviour of the ionic double layer when characterised on atomically flat gold at the electric potential of zero charge.

4.1. The physical structure of the ionic double layer on atomically flat gold

The physical structure of the double layer has been commonly divided into two regions; the inner or Stern layer [8] whose properties are presumed to be determined by a layer of solvent and solute molecules next to the metal surface, and an outer or diffuse 'Gouy-Chapmann' layer ([7,48]) in which the solvent is regarded as a uniform dielectric medium of permittivity equal to that of the bulk electrolyte, ε_{bulk} [49]. Solutions of the Boltzmann–Poisson equations yield an expression for capacitance of the outer 'Gouy-Chapmann' diffuse layer of

$$c_{Gouy\text{-}Chapmann} \equiv \frac{\varepsilon_{bulk}}{\lambda_{Debye}} \quad \text{where} \quad \lambda_{Debye} \equiv \sqrt{\frac{kT\varepsilon_{bulk}}{q^2 N_A \sum_i z_i C_i}} \tag{8}$$

where k is the Boltzmann constant, T the temperature, q the magnitude of the electronic charge, N_A Avogadro's number and C_i the concentration (in units of M m^{-3} or mM) of the ith ionic species of valence z_i comprising the electrolyte.

The theoretical 'Gouy-Chapmann' capacitance as a function of the potassium chloride concentration is plotted in Fig. 8(a). This capacitance clearly exhibits a strong dependence on concentration that is not reflected in the measured capacitance values obtained in this study for the double layer for atomically flat gold.

The region immediately adjacent to the gold surface is often referred to as the inner or "Stern" layer. This is a region where the intense electric fields (calculated to by of the order of 10^7–10^8 V m^{-1} by Verwey and Overbeek [50]) are expected to give rise to dielectric saturation of water (Stern [8] and Grahame [51]). This leads to a much reduced value for the dielectric constant of water in this region (Hasted et al. [52]). Born energies for the ions in this region with a lowered dielectric constant, give rise to ion partitioning [14] and this moderates the adsorption of ions due to attractive image forces between the ions and the metal electrode.

Theoretical estimates of the dielectric permittivity of the Stern layer is approximately 1/16th that of the bulk electrolyte [52]. Thus the dielectric geometrical capacitance per unit area of the inner Stern layer is given by

$$c_{Stern} \equiv \frac{(1/16)\varepsilon_{bulk}}{d_{Stern}} \tag{9}$$

where d_{Stern} is the thickness.

A Stern layer of thickness d_{Stern} = 6.7 Å accounts for the mean value of 0.066 F m^{-2} obtained for the average capacitance of the double layer over a substantially wide range of concentrations. This thickness is approximately twice the diameter of a potassium or chloride ion and consistent with the proposed molecular dimensions of the Stern layer. Further, our finding that the adsorption conductance was also independent of concentration of the bulk electrolyte is consistent with ions being present in the double layer at a "saturation" concentration even at the lowest electrolyte concentration of 33 μM.

5. Conclusions

Electrical impedance spectroscopy (EIS) studies of the interfacial properties of potassium chloride electrolytes in contact with rough gold surfaces and atomically flat gold surfaces formed on mica templates exhibit constant-phase-angle (CPA) dispersions of conductance and capacitance with frequency extending to very low frequencies of 6 mHz. The CPA exponent value of 0.96 obtained for the atomically flat surfaces was sufficiently close to the value of unity that renders the CPA impedance element as an "ideal capacitor" and provided realistic estimates of the capacitance of the ionic double layer at the electric potential of zero charge.

Geometrical 'fractal' models that account for surface topographies of gold–electrolyte interfaces do not predict CPA characteristics for either atomically flat surface or surfaces with mono-atomic terraces. The retention of CPA characteristics with exponents marginally less than unity is principally attributable to specific adsorption of chloride ions which was modelled as an adsorption conductance element in parallel with the CPA element.

The 'chloride' adsorption conductance values deduced for the atomically flat gold interface were independent of concentration, consistent with ion adsorption in the interface reaching saturation even at the very low electrolyte concentration of 33 μM.

The double layer capacitance values were similarly independent of the electrolyte concentration, contrary to dependencies expected for the outer diffuse 'Gouy-Chapman' region of the double layer, but consistent with electrochemical and geometrical properties proposed for the inner 'Stern' region of the interface.

Acknowledgements

The Australian Research Council funded this research (DP0452447).

Appendix A

Cantor-bar fractal model

Fig. 1 depicts the fractal model that Liu et al. ([31,32]) used to predict the *ac* response of a rough electrode in contact with an electrolyte. The electrode surface is modelled as groves W wide, L long and h high. Each grove branches into two smaller groves also of length L and height h but of a reduced width. These smaller groves branch further into two even smaller groves and so on. The overall height H of the grove is Nh where N is the number of stages of branching. The width of the grove at the nth stage of branching is given by

$$W_n = \frac{W}{a^{n-1}} \tag{A1}$$

where a is the scaling factor. The inner width of the grove is given by

$$w_n = W_n - 2W_{n+1} = W_n\left(1 - \frac{2}{a}\right) \tag{A2}$$

which is greater than zero only when

$$a > 2 \tag{A3}$$

Contributions to the impedance of the interface arise from the capacitance per unit area of the double layer, i.e. c, the conductive (σ_e) and dielectric (ε_e) properties of the electrolyte as well as the geometry of the grove shown in Fig. 3. These contributions are represented by circuit component in the equivalent circuit also shown in Fig. 2. Expressions for the capacitive components of the nth branch are

$$C_n^h = c\{2h(L + W_n)\} \tag{A4}$$

$$C_n^w = c\{2Lw_n\} \quad \text{for} \quad n < N \tag{A5}$$

$$C_N^W = c\{LW_N\} \quad \text{for} \quad n = N \tag{A6}$$

The impedance of the electrolyte in the nth branch is

$$Z_n = \frac{h}{(\sigma_e + j\omega\varepsilon_e)\{LW_n\}} \quad \text{for} \quad n < N \tag{A7}$$

where ω is the angular frequency of the applied *ac* signal (note that $\omega = 2\pi f$ where f is the frequency in units of cycles per second).

The total capacitive contribution of the nth branch is

$$C_n = C_n^h + C_n^w \quad \text{for} \quad n < N \tag{A8}$$

and that for the Nth (last) branch is

$$C_N = C_N^h + C_N^W \quad \text{for} \quad n = N \tag{A9}$$

Analysis of the equivalent circuit in Fig. 2 yields a fractal function of

$$Z(n, ZZ) \equiv Z_n + \frac{1}{j\omega C_n + (2/ZZ)} \tag{A10}$$

linking the contributions of the branches to the total impedance of the grove. The impedance of one of the groves shown in Fig. 3 with four branches is given by

$$Z_g = Z(1, Z(2, Z(3, Z(4, \infty)))) \tag{A11}$$

or with N branches

$$Z_g = Z(1, Z(\cdots Z(i, Z(\cdots Z(N-1, Z(N, \infty)))))) \tag{A12}$$

The interfacial impedance includes that of the grove (Eq. (A12)) which covers a surface area LW in parallel with that of a flat surface of equivalent area with capacitance of

$$C_W = cLW \tag{A13}$$

The interfacial impedance of area $L(2W)$ is therefore

$$Z_F = \frac{1}{j\omega C_W + (1/Z_g)} \tag{A14}$$

Measurements of the impedance between the electrolyte and the electrode utilise a reference electrode immersed in the electrolyte as shown in Fig. 1 and located a distance d from the rough surface. The impedance of the electrolyte is

$$Z_e = \frac{1}{2LW(g_e + j\omega c_e)} \quad \text{where } g_e = \frac{\sigma_e}{d} \quad \text{and} \quad c_e = \frac{\varepsilon_e}{d} \tag{A15}$$

Therefore the total impedance for the area $L(2W)$ is $Z_F + Z_e$ or the total admittance per unit area is

$$y_T \equiv g_T(\omega) + j\omega c_T(\omega) = \frac{1}{2LW(Z_F + Z_e)} \tag{A16}$$

where $g_T(\omega)$ and $c_T(\omega)$ are the equivalent parallel conductance and capacitance components, respectively, of the admittance.

In the limit of h approaching zero Eqs. (A4), (A5), (A6), (A7) and (A12) yield that

$$C_n^h \to 0,\ \ C_n^w \to 0,\ \ C_N^W \to c\{LW\},\ \ Z_n \to 0,\ \text{ and } Z_g \to \frac{1}{j\omega c\{LW\}}$$

whence Eq. (A14) simplifies to

$$Z_F(h \to 0) \to \frac{1}{j\omega c\{2LW\}} \tag{A17}$$

and Eq. (A16) simplifies to

$$y_T \equiv g_T(\omega) + j\omega c_T(\omega) \to \frac{1}{(1/j\omega c) + (1/(g_e + j\omega c_e))} \tag{A18}$$

which is, as expected, the admittance of a flat electrode in series with the electrolyte.

References

[1] H. Hillebrandt, G. Wiegand, M. Tanaka, E. Sackmann, Langmuir 15 (1999) 8451.
[2] T.C. Chilcott, E.L.S. Wong, T. Böcking, H.G.L. Coster, Physiol. Meas. 29 (2008) S307.
[3] F.-M. Boldt, N. Baltas, K. Borgwarth, J. Heinze, Surf. Sci. 59 (2005) 751.
[4] J.J. Gooding, P. Erokhin, D.B. Hibbert, Biosens. Bioelectron. 15 (2000) 229.
[5] F. Bender, T.C. Chilcott, H.G.L. Coster, D.B. Hibbert, J.J. Gooding, Electrochim. Acta 52 (2007) 2640.
[6] G. Gouy, Ann. Chim. Phys. 29 (1903) 159.
[7] D.L. Chapman, Philos. Mag. 25 (1924) 475.
[8] O. Stern, Z. Elecktrochem. 30 (1924) 508.
[9] K.S. Cole, J. Gen. Physiol. 15 (1932) 641.
[10] K.S. Cole, H.J. Curtis, J. Gen. Physiol. 21 (1938) 591.
[11] H. Fricke, Physics 1 (1931) 106.
[12] H.P. Schwan, Adv. Biol. Med. Phys. 5 (1957) 147.
[13] R. de Levie, Electrochim. Acta 10 (1965) 113.
[14] G.M. Bell, S. Levine, in: B.E. Conway, R.G. Barradas (Eds.), Chemical Physics of Ionic Solutions, Wiley, New York, 1966, p. 409.
[15] T.C. Halsey, Phys. Rev. A 35 (1987) 3512.
[16] T.C. Halsey, M. Leibig, Ann. Phys. 219 (1992) 109.
[17] W. Scheider, J. Phys. Chem. 79 (1975) 127.
[18] H.G.L. Coster, T.C. Chilcott, in: Torben Smith Sørensen (Ed.), Surface Chemistry and Electrochemistry of Membranes, Marcel Deker Inc., New York, Basel, 1999, p. 749.
[19] T. Pajkossy, Solid State Ion. 94 (1997) 123.
[20] T. Pajkossy, Solid State Ion. 176 (2005) 1997.
[21] J.B. Bates, Y.T. Chu, W.T. Stribling, Phys. Rev. Lett. 60 (7) (1988) 627.
[22] V.D. Jovíc, B.M. Jovíc, J. Electroanal. Chem. 541 (2003) 1.
[23] B.M. Jovíc, V.D. Jovíc, D.M. Drazić, J. Electroanal. Chem. 399 (1994) 197.
[24] S. Härtingher, K. Doblhofer, J. Electroanal. Chem. 380 (1995) 185.
[25] M. Sluyters-Rebach, J. Sluyters, Electroanalytical Chemistry, vol. 4, Marcel Dekker, New York, 1970, p. 75.
[26] D. Eberhardt, E. Santos, W. Schmickler, J. Electroanal. Chem. 419 (1996) 23.
[27] T. Pajkossy, T. Wandlowski, D.M. Kolb, J. Electroanal. Chem. 414 (1996) 414.
[28] J.C. Wang, J.B. Bates, Solid State Ion. 18–19 (1983) 224.
[29] A. Le Mehaute, G. Crept, Solid State Ion. 9–10 (1983) 17.
[30] M. Keddam, C.R. Takenouti, Acad. Sci. Ser. 2 (302) (1986) 281.
[31] S.H. Liu, Phys. Rev. Lett. 55 (5) (1985) 529.
[32] S.H. Liu, T. Kaplan, L.J. Gray, Solid State Ion. 18–19 (1986) 65.
[33] T. Pajkossy, J. Electroanal. Chem. 300 (1991) 1.
[34] M. Strömme, A. Gutarra, G.A. Niklasson, C.G. Granqvist, J. Appl. Phys. 79 (7) (1996) 3749.
[35] D. Losic, J.G. Shapter, J.J. Gooding, Langmuir 17 (11) (2001) 3307.
[36] H.G.L. Coster, T.C. Chilcott, "An improved method of measuring the phase difference between arbitrary periodic waveforms", PCT application filed in Australia, 2007.
[37] H.G.L. Coster, T.C. Chilcott, "Apparatus for electrochemical characterisations", PCT application 138185 filed in Australia, 2007.
[38] David R. Lide (Editor-in-Chief), CRC Handbook of Chemistry and Physics, CRC Press, 2005.
[39] J. Diebel, H. Lowe, P. Samori, J.P. Rabe, Appl. Phys. A: Mater. Sci. Process. 73 (3) (2001) 273.
[40] B. Atmaja, J. Frommer, J.C. Scott, Langmuir 22 (10) (2006) 4734.
[41] J. Mazurkiewicz, F.J. Mearns, D. Losic, L. Weeks, E.R. Waclawik, C.T. Rogers, J.G. Shapter, J.J. Gooding, J. Vac. Sci. Technol. B 20 (6) (2002) 2265.
[42] P. Samori, J. Diebel, H. Lowe, J.P. Rabe, Langmuir 15 (7) (1999) 2592.
[43] P. Wagner, M. Hegner, H.J. Guntherodt, G. Semenza, Langmuir 11 (10) (1995) 3867.
[44] C. Hinnen, C. Nguyen Van Huong, A. Rousseau, J.P. Dalbera, J. Electroanal. Chem. 95 (1979) 131.
[45] A. Hamelin, J. Electroanal. Chem. 142 (1982) 299.
[46] T.P. Moffat, in: A.J. Bard, I. Rubinstein (Eds.), Electroanalytical Chemistry: A Series of Advances, vol. 21, Marcel Dekker Inc., New York, Basel, 1999, p. 211.
[47] Z. Kerner, T. Pajkossy, J. Electroanal. Chem. 448 (1998).
[48] G. Gouy, C. R. Acad. Sci. 149 (1910) 654.
[49] D. Henderson, L. Blum, M. Lozada-Cassou, J. Electroanal. Chem. 150 (1983) 291.
[50] E.J.W. Verwey, J.T.H.G. Overbeek, "Colloids" (Elsevier) 22–34 (1948) 41.
[51] D.C. Grahame, J. Chem. Rev. 31 (1947) 441.
[52] J.B. Hasted, D.M. Riston, C.H. Collie, J. Chem. Phys. 16 (1948) 1.